Theory of optical scattering by achiral carbon nanotubes and their potential as optical nanoantennas

G. Ya. Slepyan, M. V. Shuba, and S. A. Maksimenko
Institute for Nuclear Problems, Belarus State University, Bobruiskaya 11, 220050 Minsk, Belarus

A. Lakhtakia
Department of Engineering Science and Mechanics, Pennsylvania State University, University Park, Pennsylvania 16802-6812, USA
(Received 2 January 2006; published 18 May 2006)

The Leontovich-Levin equation for optical scattering by an achiral carbon nanotube (CNT) of finite length is formulated, based on a quantum-mechanical microscopic model of the conductivity. Both approximate analytical and numerical solutions of the Leontovich-Levin equation yield a comparable surface current density distribution and scattering pattern. Applications over a wide frequency range from the terahertz to the ultraviolet are possible. The CNT polarizability in the low-frequency range and the scattering pattern in the range of optical interband transitions as well as in the vicinity of plasmon resonance are calculated. Geometric resonances of strongly retarded surface waves emerge and can be used for the qualitative interpretation of experimentally observed features in the optical response characteristics of CNT-based composite mediums. The potential of isolated CNTs as optical nanoantennas of both the receiving and transmitting types is established.

DOI: 10.1103/PhysRevB.73.195416 PACS number(s): 73.25.+i, 42.70.−a, 78.67.Ch, 77.84.Lf

I. INTRODUCTION

Among a variety of different nanostructures, quasi-one-dimensional carbon macromolecules called carbon nanotubes[1] (CNTs) are the subject of intense research worldwide—largely because of their unique electronic properties. It is well known that, depending on the radius and folding of the graphite monolayer forming a CNT, it displays either metallic or semiconducting properties.[2,3] Naturally, their folding geometry and unusual electronic transport properties dictate the specific features of the interactions of CNTs with electromagnetic waves. Interesting examples of such interactions are (i) strongly retarded surface waves,[4–6] (ii) modification of the density of photonic states in the vicinity of a CNT,[7] (iii) highly efficient generation of high-order harmonics,[8–10] and (iv) the possibility of CNT-based terahertz emitters.[11–13]

An intriguing electromagnetic problem of nanoscience is the realization of nanoscale antennas for infrared and visible light. Such an antenna would allow a very desirable modality of communications between nanoelectronic devices and the macroscopic world.

Already, various physical principles underlying optical antennas have been offered[14–16] and the idea of CNT nanoantennas is definitely attractive.[17–23] Recently, nanoantenna operation of a CNT array was demonstrated experimentally.[24] CNTs offer control of the polarization state, radiation pattern, gain, and other characteristics.[21] No wonder, the application of CNTs as microwave antennas has been suggested,[20] based on electrically connected single-walled CNTs up to 1 cm in length.[25,26] Of course, care must be exercised because CNTs are not necessarily perfect conductors, unlike wire antennas.[17]

Until recently, as virtually a general rule, the electromagnetic properties of CNTs were modeled under the assumption of the nanotubes being infinitely long, thereby neglecting the edge effects.[17] But *edge effects crucially determine antenna properties*. Moreover, the infinite-length assumption restricts the applicability of theoretical results to modeling of the electromagnetic response properties of CNT ensembles, which are effectively homogeneous mediums at sufficiently low frequencies.[27–29] At optical frequencies, the lengths of actual CNTs are comparable to the (free-space) wavelength; consequently, the polarizability tensors of CNTs—which are necessary for estimation of the effective constitutive parameters of CNT ensembles—are gravely and adversely affected by the infinite-length assumption.

Thus, the problem of electromagnetic-wave scattering by an isolated CNT of finite length must be considered a canonical problem of nanoelectromagnetics. This canonical problem must be tackled for understanding the potentiality of as well as for designing CNT nanoantennas.

The role of edge effects in the electromagnetic responses of isolated semi-infinite CNTs was investigated earlier[17] using the Wiener-Hopf technique (also called the factorization method).[30,31] But the extension of the Wiener-Hopf technique to finite-length structures is unfruitful—as discussed by Mittra and Lee[31] —because it does not lead to exact analytical formulas. Therefore, direct analysis based on the integral equations of electromagnetics is appealing, which conclusion provided the motivation for this paper.

Since the cross-sectional radius of a CNT is much smaller the wavelength in the optical regime, whereas the CNT length is comparable in magnitude, by virtue of the scale invariance of the Maxwell equations,[32–34] microwave wire antennas can serve as macroscopic analogs of CNTs in the optical regime. An adequate theory of isolated wire antennas has been developed from an integral equation by Leontovich and Levin.[35] Although that method is suitable for CNTs, its direct application to CNTs in the optical regime is impossible

for two reasons. First, to a high accuracy, microwave wire antennas are virtually perfect conductors,[35] which underlies the Lentovich-Levin method. Accounting for the skin effect modifies, but does not significantly change, the application of the Leontovich-Levin method. In contrast, the conductivity of a CNT is influenced by interband transitions and thus demonstrates complex resonances in the optical regime.[4,6] Second, the effective boundary conditions on the electromagnetic field on the surface of a CNT—which are two-sided impedance boundary conditions[4,6] used in macroscopic electromagnetics for the characterization of semitransparent grid screens[30]—are nontrivially different from those for microwave wire antennas. Therefore, standard approaches for microwave wire antennas require modification for application to CNT optical nanoantennas.

To our knowledge, there are just two theoretical treatments of CNT antennas available.[20,23] The treatment of Burke *et al.*[20] contains two basic restrictions. First, it is based on the telegrapher's equations: hence, as it neglects the influence of radiation on the current distribution, it is not self-consistent. The assumption is often used for macroscopic wire antenna,[36] but its application to CNT antennas appears dubious. This is because the working modes of a microwave wire antenna and a CNT optical nanoantenna are essentially different: Transverse electromagnetic (TEM) modes propagate in macroscopic vibrators, whereas strongly retarded surface waves are characteristic of CNTs.[4,6] Therefore the CNT conductivity and inductance per unit length must be derived from electronic transport characteristics of CNTs and incorporated into the treatment of Burke *et al.* Second, as that treatment[20] does not take into account interband transitions of π electrons, its applicability is limited to the low-frequency regime below the optical (interband) transition threshold.

A better approach to CNT nanoantennas has recently been developed by Hanson[23] as the numerical solution of the Hallén integral equation[37,38] with effective two-side impedance boundary conditions.[4] However, interband transitions are again beyond the pale of this treatment, which is therefore restricted to the low-frequency regime. But in that regime, a CNT behaves similarly to a point dipole antenna,[38] and so its radiative pattern has a trivial dependence on the scattering angle: $F(\theta) \sim \sin\theta$.

We present here a self-consistent theoretical analysis of scattering by an arbitrary achiral CNT in a wide frequency range, from terahertz up to ultraviolet frequencies. Our analysis is free of the restrictions accompanying its predecessor treatments.[20,23]

This paper is organized as follows. In Sec. II, the Leontovich-Levin equation is formulated for an isolated CNT of finite length. In Sec. III, an approximate analytical solution of that integral equation is found as the first step in an iterative procedure. The scattering of plane waves by a finite-length CNT is analyzed in a wide range of frequencies and angles of incidence in Sec. IV, with ensuing discussions provided in Sec. V. Numerical and approximate analytical solutions are compared, and the paper concludes in Sec. VI with an assessment of both resonances in CNT-based composite media and an isolated CNT as an optical nanoantenna.

II. INTEGRO-DIFFERENTIAL EQUATIONS FOR A FINITE-LENGTH CNT

A. Boundary-value problem

Let an isolated single-walled CNT of length L and cross-sectional radius R, and aligned parallel to the z axis of a Cartesian coordinate system, be exposed to an externally impressed field $\mathbf{E}_{\text{inc}}(\mathbf{r},t)=\mathbf{E}_0(\mathbf{r})\exp(-i\omega t)$, where ω is the angular frequency. This fields induces a surface current density $\mathbf{j}(\mathbf{r})$ in the CNT, which reradiates the scattered field.

The scattered electromagnetic field can be expressed in terms of the electric Hertz potential Π,[30] such that

$$(\nabla^2 + k^2)\Pi = 0, \tag{1}$$

where $k=\omega/c$ is the free-space wave number and c is speed of light in vacuum.

Assuming the CNT radius to be small as compared to the free-space wavelength $\lambda=2\pi/k$, we neglect the transverse current—that is, we set $\mathbf{j}(\mathbf{r})=j(\mathbf{r})\mathbf{e}_z$, where $\mathbf{e}_z$ is the unit vector along the CNT axis. Furthermore, we set $j(\mathbf{r})=j(z)$, thereby neglecting other spatial variations of the axial current on the CNT surface. Hence, in the cylindrical coordinate system (ρ,z,ϕ), we get

$$\Pi(\mathbf{r}) \equiv \Pi(\rho,z)\mathbf{e}_z. \tag{2}$$

Accordingly, the only nonzero components of the scattered electromagnetic fields are as follows:

$$E_\rho^{\text{sc}} = \frac{\partial^2\Pi}{\partial z\,\partial\rho}, \tag{3}$$

$$E_z^{\text{sc}} = \left(\frac{\partial^2}{\partial z^2} + k^2\right)\Pi, \tag{4}$$

$$H_\phi^{\text{sc}} = ik\frac{\partial\Pi}{\partial\rho}. \tag{5}$$

Three boundary conditions for (1) emerge from the effective impedance boundary conditions for CNTs (Ref. 4) as follows:

$$\left.\frac{\partial\Pi}{\partial\rho}\right|_{\rho=R+0} - \left.\frac{\partial\Pi}{\partial\rho}\right|_{\rho=R-0} = \frac{4\pi\sigma_{zz}}{ikc}\left[\frac{\partial^2\Pi}{\partial z^2} + k^2\Pi + E_{0z}\right], \quad |z| < L/2, \tag{6}$$

$$\left.\frac{\partial\Pi}{\partial\rho}\right|_{\rho=R+0} = \left.\frac{\partial\Pi}{\partial\rho}\right|_{\rho=R-0}, \quad |z| > L/2, \tag{7}$$

$$\Pi|_{\rho=R+0} = \Pi|_{\rho=R-0}, \quad -\infty < z < \infty. \tag{8}$$

Here and hereafter, $E_{0z}=\mathbf{E}_0\cdot\mathbf{e}_z$ and σ_{zz} is the axial conductivity of an isolated CNT.

The boundary conditions (6)–(8) actually hold for infinitely long CNTs.[4] But these conditions are local and there-

fore can be applied to finite-length CNTs and other finite objects such as smooth joints of CNTs of different radii, Y junctions of CNTs, and CNT ensembles. The situation is the same as in the theory of the skin effect in three-dimensional (3D) bulk conductors: although impedance boundary conditions are derived for plane infinite surfaces, they are generalized to finite bodies with curved surfaces, waveguides, gratings, etc. A negligibly small skin depth in comparison to the typical body size and radius of curvature is the necessary condition for the approach to be valid.[39] For CNTs the boundary conditions (6)–(8) remain local if the condition $L \gg R$ holds true.

The presence of edges modifies the electron zone structure in CNTs due to the electron edge states.[40] There are two types of edge states. The first type are due to the direct influence of the edges in strict analogy with the Tamm levels in semi-infinite bulk mediums, and the second type are due to topological defects such as pentagons in a hexagonal carbon lattice. Since the edge states of both types are strongly localized in the vicinity of the edges,[40] we neglected their contribution to the CNT conductivity. However, we do take the edges into account in Sec. II C and later.

B. Axial conductivity

The axial conductivity σ_{zz} was derived via quantum transport theory as[6]

$$\sigma_{zz}(\omega) = -\frac{ie^2\omega}{\pi^2 \hbar R}\left\{\frac{1}{\omega(\omega + i/\tau)}\sum_{s=1}^{m}\int_{1\text{st BZ}}\frac{\partial F_c}{\partial p_z}\frac{\partial \mathcal{E}_c}{\partial p_z}dp_z - 2\sum_{s=1}^{m}\int_{1\text{st BZ}}\mathcal{E}_c|R_{vc}|^2\frac{F_c - F_v}{\hbar^2\omega(\omega + i/\tau) - 4\mathcal{E}_c^2}dp_z\right\}, \tag{9}$$

where e is the electron charge, $\hbar$ is the normalized Planck constant, and p_z is the axial projection of quasimomentum. The integer $s=1,2,3,\ldots,m$ labels the π-electron energy bands; here, m is an index appearing in the dual index (m,n) used to classify CNTs.[3,5,6] The time constant of the electronic mean free path τ is assumed to be equal to the inverse relaxation frequency.

The first term on the right side of (9) is the Drude term corresponding to the intraband conductivity, while the second term describes the contribution of interband transitions between the valence and conduction bands. The indexes c and v refer to the conduction and valence bands, respectively.

The abbreviation "1st BZ" restricts the variable p_z to the first Brillouin zone, and

$$F_{c,v}(p_z,s) = \frac{1}{1 + \exp\left[\dfrac{\mathcal{E}_{c,v}(p_z,s) - \mu_{\text{ch}}}{k_B T}\right]} \tag{10}$$

is the equilibrium Fermi distribution function. Here T is the temperature, k_B is the Boltzmann constant, and μ_{ch} is the chemical potential; in graphite and undoped CNTs, $\mu_{\text{ch}}=0$.

The normalized matrix elements of the dipole transition between conduction and valence bands, denoted by R_{vc}, are evaluated in the tight-binding approximation after taking into account transverse quantization of the charge carriers' motion and the hexagonal structure of the graphene lattice.[6,10] For zigzag CNTs, which are denoted by the dual index $(m,0)$, we have

$$R_{vc}(p_z,s) = -\frac{b\gamma_0^2}{2\mathcal{E}_c^2(p_z,s)}\left[1 + \cos(ap_z)\cos\left(\frac{\pi s}{m}\right) - 2\cos^2\left(\frac{\pi s}{m}\right)\right], \tag{11}$$

where $b=0.142$ nm is the interatomic distance in graphene, $\gamma_0 \approx 2.7$ eV is the overlap integral,[41] and $a=3b/2\hbar$. The electron energy for zigzag nanotubes is given by[3]

$$\mathcal{E}_{c,v} = \pm\,\gamma_0\sqrt{1 + 4\cos(ap_z)\cos\left(\frac{\pi s}{m}\right) + 4\cos^2\left(\frac{\pi s}{m}\right)}, \tag{12}$$

and explicit expressions for $\mathcal{E}_{c,v}$ and R_{vc} for armchair (m,m) CNTs are also known.[3]

C. Edge conditions

The boundary conditions (6)–(8) have to be supplemented by radiation conditions[30] as well by edge conditions. The latter express the absence of the concentrated charges on the edges $z=\pm L/2$ of the (Ref. 30)—i.e.,

$$j(\pm L/2) = 0. \tag{13}$$

D. Hallén equation for a CNT

Since the axial current in the CNT is assumed to be independent of the azimuthal coordinate, we can formulate an approximate 1D integro-differential equation which is tractable both for numerical work and approximate analytical solution.

In the theory of microwave wire antennas, there are different methods for that averaging. Each method leads to a specific form of the 1D integrodifferential equation: the Leontovich-Levin equation,[35] the Hallén equation,[37,38] the Pocklington equation,[42,43] etc. Although these equations are physically equivalent to one another, their specific forms make them suitable for different problems. We chose the Leontovich-Levin equation[35] for application to CNTs, because it is amenable to both analytical and numerical methods at different stages of analysis.

The solution of the Helmholtz equation (1) with boundary conditions (6)–(8) and edge conditions (13) is sought as a single-layer potential—i.e.,

$$\Pi(\rho,z) = \frac{2iR}{\omega}\int_0^{\pi}\int_{-L/2}^{L/2} j(z')G(R,\rho,\phi,z-z')dz'd\phi, \tag{14}$$

where $j(z)$ is the unknown surface current density to be found and

$$G(R,\rho,\phi,z) = \frac{\exp[ik\sqrt{R^2+\rho^2-2R\rho\cos\phi+z^2}]}{\sqrt{R^2+\rho^2-2R\rho\cos\phi+z^2}} \quad (15)$$

is the free-space Green function. In view of the continuity of the single-layer potential over the whole space including the CNT surface, the boundary conditions (7) and (8) are fulfilled automatically, whereas the boundary condition (6) gives

$$j(z) = \sigma_{zz}\left[\frac{\partial^2\Pi(R,z)}{\partial z^2} + k^2\Pi(R,z) + E_{0z}(z)\right]. \quad (16)$$

On the nanotube surface ($\rho=R$), the Green function in (14) can be rewritten as

$$G(R,R,\phi,z-z') = G(\phi,z-z') = \exp(ikr)/r, \quad (17)$$

with $r=\sqrt{(z-z')^2+\zeta^2}$ and $\zeta=2R\sin(\phi/2)$.

Next we define

$$\tilde{\Pi}(z) = \Pi(R,z) + \Phi(z), \quad (18)$$

where

$$\Phi(z) = \frac{1}{2ik}\int_{-L/2}^{L/2} E_{0z}(z')\exp(ik|z-z'|)dz' + C_1\exp(ikz) + C_2\exp(-ikz), \quad (19)$$

with C_1 and C_2 as arbitrary constants. In terms of $\tilde{\Pi}(z)$, the surface current density is expressed as

$$j(z) = \sigma_{zz}\left[\frac{\partial^2\tilde{\Pi}(z)}{\partial z^2} + k^2\tilde{\Pi}(z)\right]. \quad (20)$$

Substitution of (18) and (20) into (14) leads to the Hallén equation

$$\tilde{\Pi}(z) - \Phi(z) = \frac{2i\sigma_{zz}R}{\omega}\int_0^{\pi}\int_{-L/2}^{L/2}\left[\frac{\partial^2\tilde{\Pi}(z')}{\partial z'^2} + k^2\tilde{\Pi}(z')\right]G(\phi,z-z')dz'd\phi. \quad (21)$$

If we find the Hertz potential from the foregoing equation, Eq. (20) allows us to obtain the surface current distribution over the CNT.

The Hallén equation for CNTs was first derived and numerically solved by Hanson.[23] The integral in (21) can be handled by a quadrature formula, thereby transforming (21) into a matrix equation. The solution of the corresponding characteristic equation yields the eigenfrequencies and eigenmodes of a CNT as a high-Q microcavity.

E. Leontovich-Levin equation for a CNT

For further analysis, we consider the inner integral in Eq. (21):

$$\tilde{T}(z,\phi) = \int_{-L/2}^{L/2}\frac{j(z')}{r}\exp(ikr)dz'. \quad (22)$$

Here, $z'=z\pm\sqrt{r^2-\zeta^2}$ and $dz'=\pm rdr/\sqrt{r^2-\zeta^2}$, where the upper and lower signs correspond to the regions $z'>z$ and $z'<z$, respectively. As such, $\tilde{T}(z,\phi)$ can be rewritten as

$$\tilde{T}(z,\phi) = -\int_{z'=-L/2}^{z'=z}\frac{j(z')\exp(ikr)}{\sqrt{r^2-\zeta^2}}dr + \int_{z'=z}^{z'=L/2}\frac{j(z')\exp(ikr)}{\sqrt{r^2-\zeta^2}}dr. \quad (23)$$

In view of the condition (13) and the identity $dr/\sqrt{r^2-\zeta^2} = d\ln[q(r+\sqrt{r^2-\zeta^2})]$ with q as an arbitrary constant with the dimensionality of the inverse length, integration by parts leads to

$$\tilde{T}(z,\phi) = -2j(z)\exp(ik\zeta)\ln(q\zeta) + \int_{-L/2}^{L/2}\ln[q(r+\sqrt{r^2-\zeta^2})]\exp(ikr) \times\left[\frac{z-z'}{|z-z'|}\frac{\partial j(z')}{\partial z'} - ikj(z')\frac{|z-z'|}{r}\right]dz'. \quad (24)$$

On the CNT surface the inequality $k\zeta \ll 1$ holds true, which allows us to exploit the following approximations: $r+\sqrt{r^2-\zeta^2}\approx 2|z'-z|$ and $r\approx|z'-z|$. Then, correct to order kR, we have

$$\tilde{T}(z,\phi) = -2j(z)\ln(q\zeta) + V[z,j(z)], \quad (25)$$

where

$$V[z,j(z)] = \int_{-L/2}^{L/2}\ln(2q|z-z'|)\exp(ik|z-z'|) \times\left[\frac{z-z'}{|z-z'|}\frac{\partial j(z')}{\partial z'} - ikj(z')\right]dz'. \quad (26)$$

Subject to (20), substitution of (25) into (21) followed by integration over the azimuthal coordinate ϕ leads to the integrodifferential equation

$$\left[\frac{\partial^2}{\partial z^2} + \left(k^2 - \frac{i\omega}{2\pi\sigma_{zz}RX}\right)\right]\tilde{\Pi}(z) = -\frac{i\omega}{2\pi\sigma_{zz}RX}\Phi(z) + \frac{1}{\sigma_{zz}X}V[z,j(z)], \quad (27)$$

where

$$X = 2\ln(2qR) + \frac{2}{\pi}\int_0^{\pi}\ln[\sin(\phi/2)]d\phi = 2\ln(qR). \quad (28)$$

Equation (27) includes the arbitrary parameter q. It is reasonable to choose q in such a way as to minimize the contribution of the integral $V[z,j(z)]$ in (27). For this purpose,

we assume that the eigenfunctions of the differential operator on the left side of (27) are identical to the eigenwaves in a transmission line.

In the case of a perfectly conducting wire antenna, the eigenfunctions are the forward and counterpropagating T waves of a single-wire transmission line;[30] hence, it is sufficient to set $q=k$ (Ref. 35).

But the situation is radically different for a CNT in the optical regime, because the eigenwaves in a CNT are strongly retarded surface waves.[4] From the differential operator on the right side of (27), we find the corresponding complex-valued wave numbers

$$\kappa = \pm \sqrt{k^2 - i\omega/(2\pi\sigma_{zz}RX)}. \tag{29}$$

An alternative expression for these wave numbers emerges from a dispersion equation as[4]

$$\kappa^2 = k^2 + \frac{i\omega}{4\pi R\sigma_{zz}K_0(\sqrt{\kappa^2 - k^2}R)I_0(\sqrt{\kappa^2 - k^2}R)}, \tag{30}$$

where $K_0(\cdot)$ and $I_0(\cdot)$ are the modified Bessel functions. Then, X can be obtained from the two foregoing equations as

$$X = -2K_0(\sqrt{\kappa^2 - k^2}R)I_0(\sqrt{\kappa^2 - k^2}R) \tag{31}$$

and, correspondingly,

$$q = R^{-1}\exp(X/2). \tag{32}$$

Now, let us apply the operator $(\partial^2/\partial z^2 + k^2)$ to the right and left sides of (27). Then, in view of (20), Eq. (27) transforms into the integrodifferential equation

$$\left[\frac{\partial^2}{\partial z^2} + \left(k^2 - \frac{i\omega}{2\pi\sigma_{zz}RX}\right)\right] j(z) = -\frac{i\omega}{2\pi RX}E_{0z}(z) + \frac{1}{X}\left(\frac{\partial^2}{\partial z^2} + k^2\right) V[z, j(z)] \tag{33}$$

for the axial current density in the CNT.

Equation (33) is the Leontovich-Levin equation for a CNT in the optical regime. Its solution must take the boundary conditions (13) into account. The first term on the right side of (33) describes the action of the externally impressed field, while the second term is due to the influence of the current distribution over the CNT. As $\sigma_{zz} \to \infty$, Eq. (33) reduces to the Leontovich-Levin equation for a perfectly conducting thin-wire antenna.[35]

III. APPROXIMATE ANALYTICAL SOLUTION

Let us now obtain an approximate analytical solution of (33) with an iterative approach. Since the quantity $1/X$ determined by (31) is a small parameter as compared with unity, the axial current density in (33) may be expanded as the series

$$j(z) = j^{(0)}(z) + \frac{1}{X}j^{(1)}(z) + \frac{1}{X^2}j^{(2)}(z) + \cdots . \tag{34}$$

The zeroth-order approximation $j^{(0)}(z)$ satisfies the equation

$$\frac{\partial^2 j^{(0)}(z)}{\partial z^2} + \left(k^2 - \frac{i\omega}{2\pi\sigma_{zz}RX}\right) j^{(0)}(z) = -\frac{i\omega}{2\pi RX}E_{0z}(z), \tag{35}$$

whereas the ℓth-order term ($\ell > 0$) can be obtained from the recurrence relation

$$\left[\frac{\partial^2}{\partial z^2} + \left(k^2 - \frac{i\omega}{2\pi\sigma_{zz}RX}\right)\right] j^{(\ell)}(z) = \left(\frac{\partial^2}{\partial z^2} + k^2\right) V[z, j^{(\ell-1)}(z)]. \tag{36}$$

In the zeroth-order approximation we neglect all terms in (34) except the first one, so that

$$j(z) \simeq j^{(0)}(z). \tag{37}$$

Thus, we neglect the influence of radiation on the current distribution over the CNT, the relatively small impact of this neglect being demonstrated in Sec. IV by comparing the predictions due to (37) with those obtained by direct numerical solution of the Hallén equation (21).

The result obtained resembles that from the transmission-line model formulated by Burke *et al.*[20] for a CNT dipole antenna. But that formulation is not self-consistent. Indeed, (35) can be reduced to the standard form of the telegrapher's equations with circuit parameters per unit length expressed in terms of X and σ_{zz}. However, the values of circuit parameters evaluated in that way turn out to be significantly different from the corresponding parameters in Ref. 20. The reason for the differences is as follows. The formulation of Burke *et al.* is based on the intuitive assumption that the retarded wave in a CNT is constituted by π electrons at the Fermi level. Therefore, the phase velocity in CNT turns out to be of the order of the Fermi velocity $v \simeq v_F$ (Ref. 44), which corresponds to the retardation $v/c \simeq 0.01$. A more rigorous analysis[4,6] demonstrates that the contribution of other energy levels is also of significance and a more realistic estimate of the retardation is $v/c \simeq 0.02$. Thus, the theory presented in Ref. 20 allows an estimation of the qualitative characteristics of a CNT antenna, but it may lead to incorrect spectral features. The same conclusion has been arrived at by Hanson[23] from numerical analysis.

The inequality

$$k^2 \ll \frac{\omega}{|2\pi\sigma_{zz}RX|} \tag{38}$$

holds true for both semiconducting and metallic CNTs in a wide frequency range from terahertz to ultraviolet, except in the vicinity of the plasmon resonance.[45] We define the plasmon resonance as the frequency[46]

$$\omega_p = 2\gamma_0/\hbar, \tag{39}$$

and CNTs satisfying condition (38) are referred to as *impedance* CNTs from here onwards. The electric current density in the CNT is derived from (35) with boundary condition (13) as

$$j(z) = D_+ \exp(i\kappa z) + D_- \exp(-i\kappa z) + \frac{\sigma_{zz}(\kappa^2 - k^2)}{2i\kappa} \times \int_{-L/2}^{L/2} E_{0z}(z') \exp(i\kappa |z - z'|) dz', \quad (40)$$

where

$$D_\pm = \frac{f_\mp - f_\pm \exp(-i\kappa L)}{[\exp(-2i\kappa L) - 1]} \quad (41)$$

and

$$f_\pm = \frac{\sigma_{zz}(\kappa^2 - k^2)}{2i\kappa} \int_{-L/2}^{L/2} E_{0z}(z') \exp(\pm i\kappa z') dz'. \quad (42)$$

The first two terms on the right side of (40) describe strongly retarded surface waves with wave number $\kappa' = \mathrm{Re}(\kappa)$ and damping constant $\kappa'' = \mathrm{Im}(\kappa)$.

When $\kappa' \gg \kappa''$, these surface waves are weakly attenuated; hence, there are surface-wave resonances at frequencies related to the CNT length by the condition

$$\kappa'(\omega) L \approx \pi s, \quad s = 1, 2, \ldots . \quad (43)$$

Note that this definition differs from the terminology adopted in Refs. 20 and 23, wherein surface-wave resonances determined by the condition (43) are referred to as *plasmon resonances*. Since they are determined solely by the geometry of CNTs, we prefer to call the surface-wave resonances as *geometric resonances*. In the vicinity of these resonances, the surface current density is mainly determined by first two terms on the right side of (40).

When $\kappa' \approx \kappa''$, the surface wave rapidly attenuates on the CNT. The current density distribution in the central part of nanotube is then determined by the third term on the right side of (40) and thus follows the external field distribution—because the accompanying first and second terms contribute significantly only in the vicinity of CNT edges $z = \pm L/2$. In Sec. IV, a comparison of the approximate analytical solution (40) with the numerical results presented by Hanson[23] shows that (40) is a quite reasonable approximation for both semiconducting and metallic nanotubes.

Knowledge of the surface current density distribution allows determination of the scattered electromagnetic field in far zone in polar coordinates as[36]

$$E_\theta^{sc}(r, \theta) = H_\phi^{sc}(r, \theta) = -\frac{2i\pi\omega RL}{c^2} \frac{\exp(ikr)}{r} F(\theta), \quad (44)$$

where $r = \sqrt{\rho^2 + z^2}$ and $\theta = \tan^{-1}(\rho/z)$, and

$$F(\theta) = \frac{\sin\theta}{L} \int_{-L/2}^{L/2} j(z) \exp(-ikz \cos\theta) dz \quad (45)$$

is the *scattering pattern*.

Let a plane wave $\mathbf{e}_p \exp(i\mathbf{k}\cdot\mathbf{r} - i\omega t)$ be incident on a CNT such that $\mathbf{k}\cdot\mathbf{e}_z = k\cos\theta_0$ and $\mathbf{e}_p = \mathbf{k}\times(\mathbf{k}\times\mathbf{e}_z)/k^2$. In this case, the scattering pattern is given by

$$F(\theta, \theta_0) \equiv F(\theta) = A\tilde{f}[(\cos\theta_0 - \cos\theta)kL/2] + B_+\tilde{f}[(k\cos\theta - \kappa)L/2] + B_-\tilde{f}[(k\cos\theta + \kappa)L/2], \quad (46)$$

where

$$\tilde{f}(\xi) = \frac{\sin\xi}{\xi}, \quad (47)$$

$$A = \sigma_{zz} \sin\theta_0 \frac{\kappa^2 - k^2}{(\kappa^2 - k^2\cos^2\theta_0)}, \quad (48)$$

and

$$B_\pm = -A \frac{\sin[(\kappa \pm k\cos\theta_0)L/2]}{\sin(\kappa L)}. \quad (49)$$

Equation (46) satisfies the reciprocity theorem $F(\theta, \theta_0) = F(\theta_0, \theta)$.

In the long-wavelength regime ($L \ll \lambda$), the electromagnetic properties of a CNT can be characterized by the polarizability scalar

$$\alpha = \frac{2\pi i R}{\omega} \int_{-L/2}^{L/2} j(z) dz, \quad (50)$$

and the scattering pattern is the same as for an electrically small, dipolar scatterer.[47]

IV. NUMERICAL RESULTS

A. Frequency range of optical transitions

Numerical studies were initially undertaken for the (9,0) zigzag CNT, with $\tau = 3 \times 10^{-12}$ s (Ref. 48). In the frequency regime of optical transitions (i.e., from near-infrared to ultraviolet), κ'' is sufficiently large and surface waves are strongly attenuated. Thus, as mentioned in Sec. III, in this regime the surface current density distribution is described by (40) reasonably well and the scattering pattern is given by (46). The scattering pattern of an electrically long CNT ($L \gg 1/\kappa''$) is mainly determined by the third term in expression (46), whereas the first and second terms are significant only near the CNTs edges—as is evident from Fig. 1. Clearly then, the first and second terms on the right side of (40) are significant only for short CNTs ($L \ll 1/\kappa''$).

Figure 2 demonstrates the changes in the scattering pattern with the CNT length and the angle of incidence. Figures 2(a) and 2(b) indicate that the main lobe narrows and becomes more pronounces as L increases. As follows from (46), the maximum of the main lobe is observed at the angle $\theta = \theta_0$. Therefore, the main lobe rotates and new minor lobes appear with the change of θ_0, which is evident from Figs. 2(a) and 2(c). Equation (46) predicts increase in the scattered intensity in the vicinity of interband transitions, where σ_{zz} increases drastically.

Figure 3 depicts the scattering patterns for zigzag CNTs at the plasmon frequency and different mean-free-path time constants. Figures 3(a) and 3(b) are drawn for $\theta_0 = 90°$ and

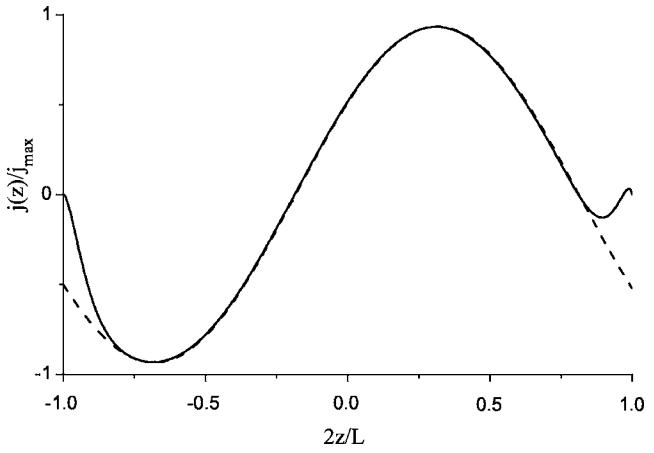

FIG. 1. Normalized distribution of axial current density $j(z)/j_{\max}$ on a $(9,0)$ zigzag CNT of length $L=1.16\lambda$, in the frequency regime of optical transitions (solid line), when $\theta_0=30°$ and $\lambda=432.4$ nm. For comparison, the distribution in an infinitely long CNT, $j(z)=\sigma_{zz}E_{0z}(z)$, is presented as the dashed line.

$\theta_0=55°$, respectively. A CNT with even m (=18) was chosen, because the conductivity of $(2l,0)$ zigzag tubes in the vicinity of plasmon frequency is 10–100 times larger (dependent on the mean free pass time magnitude) than the conductivity of other achiral CNTs, armchair or zigzag, with odd m. That property follows from the fact that $\mathcal{E}_{c,v}(p_z,m/2)=\pm\gamma_0$ for any even m; see (12). Therefore, in zigzag CNTs with even m, the band gap for π electrons $\mathcal{E}_c-\mathcal{E}_v=2\gamma_0$ is constant over the entire Brillouin zone and is equal to the plasmon energy

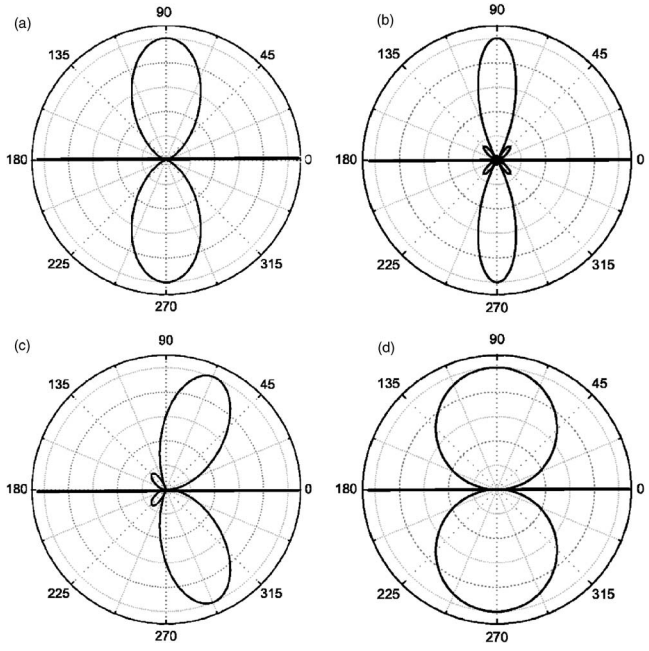

FIG. 2. Scattering patterns for a $(9,0)$ zigzag CNT in the frequency regime of optical transitions for different values of L and θ_0, when $\lambda=432.4$ nm. (a) and (c) $L=\lambda$, (b) $L=2\lambda$, (a) and (b) $\theta_0=90$, and (c) $\theta_0=60°$. The scattering pattern in the long-wavelength limit $L\ll\lambda$ is presented in (d). The horizontal bold lines show the orientation of the CNT.

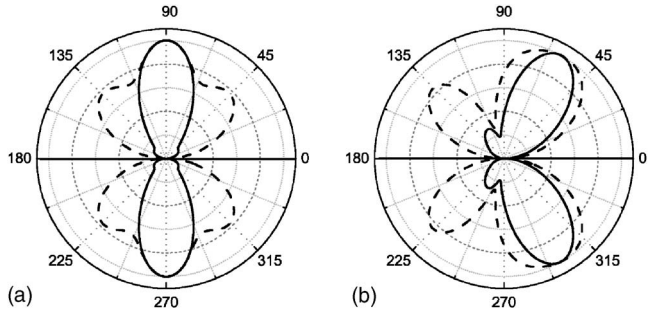

FIG. 3. Scattering patterns for a $(18,0)$ zigzag CNT of length $L=1.4\lambda$ at the plasmon frequency ω_p. Solid and dashed lines correspond to $\tau=1\times10^{-12}$ s and $\tau=1\times10^{-11}$ s, respectively, and $\lambda=432.4$ nm. (a) $\theta_0=90°$ and (b) $\theta_0=55°$.

$\hbar\omega_p=2\gamma_0$. In other words, *all* electrons in the Brillouin zone are resonant. The contribution of these resonant electrons to σ_{zz}, as described by the term with $s=m/2$ in the second sum on the right side of (9), becomes dominantly large. Thus, for large τ, the scattering patterns of $(2l,0)$ CNTs turn out to be similar to those for perfectly conducting wire antennas, as is confirmed by the dashed lines in Fig. 3. A decrease in τ changes the patterns to the form characteristic for high-impedance wire antennas; see the solid lines in Fig. 3. We have observed that the same behavior in the vicinity of the plasmon frequency is characteristic of other achiral CNTs.

Parenthetically, the special attributes of the scattering patterns of $(2l,0)$ zigzag CNTs in the vicinity of the plasmon frequency as functions of τ should be useful for the experimental determination of τ and the CNT type.

B. Long-wavelength regime

Figure 4 presents spectral dependences of the real and imaginary parts of the polarizability scalar α of a (9,0) zigzag CNT far below the frequency range of interband optical transitions—i.e., in the long-wavelength regime ($L\ll\lambda$). The dashed line corresponds to the approximate analytical solution (40), while the solid line is for the numerical solution of (21) by a method analogous to that of Hanson.[23]

Resonances of the polarizability scalar occur in Fig. 4 at frequencies satisfying (43). The resonance modes are subdivided into symmetric (s odd) and antisymmetric (s even) types. Antisymmetric modes give minor contributions to α, because the contributions of different regions of the CNT to the integral (44) cancel out. As s increases from unity, the resonances of α become less pronounced.

The dotted line in Fig. 4(b) shows the polarizability of a perfectly conducting nanotube. Obviously, a CNT is not a perfect conductor—neither at low frequencies nor off-resonance.

The polarizability scalar of semiconducting CNTs also demonstrates resonant behavior with resonances redshifted in comparison to metallic CNTs. The eigenwaves excited in semiconducting CNTs have extremely strong retardation $v/c\simeq1.8\times10^{-4}$ and therefore contribute to the low-frequency polarizability scalar. As an example, Fig. 5 demonstrates the geometric resonance of α at linear frequency

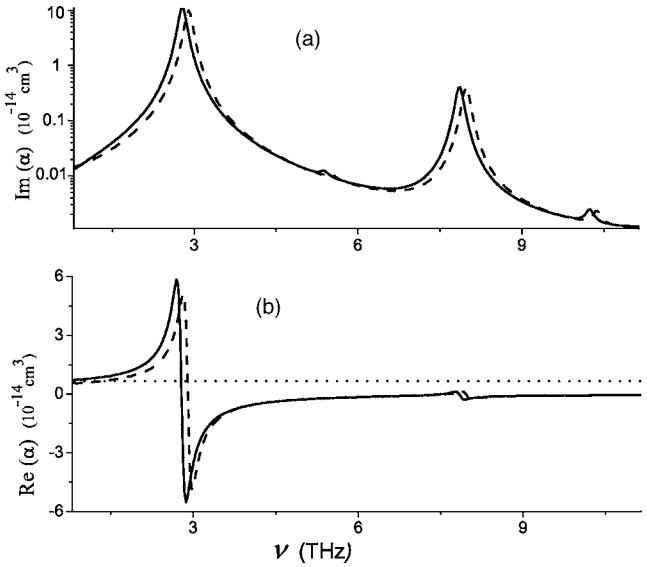

FIG. 4. Frequency dependences of (a) the imaginary and (b) real parts of the polarizability scalar α of a (9,0) zigzag metallic CNT of length $L=1$ μm. The solid line presents the exact numerical solution, while the dashed line corresponds to the approximate analytical solution (40). The polarizability scalar of a perfectly conducting nanotube is depicted by the dotted line.

$\nu=\omega/2\pi=25$ GHz for a (23,0) semiconducting zigzag CNT of length $L=1000$ nm. Obviously, the corresponding free-space wavelength considerably exceeds the CNT length. Since surface waves formed on semiconducting CNTs possess higher retardation and higher attenuation, geometric resonances in such nanotubes are shifted into the GHz regime.

Strong retardation of electromagnetic waves is characteristic of various types of nanostructures. For example, Refs. 49 and 50 predict additional geometric resonances (Mie resonances) in the vicinity of the exciton line of a semiconductor spherical quantum dot (QD), where the Lorentzian form for the effective permittivity of a composite medium containing QD's holds. As a result, the wavelength in the composite medium becomes comparable to the linear dimensions of the QD's, thereby providing strong amplification in the regime $kR_{QD} \ll 1$ where R_{QD} is the QD radius. Note that the retardation of electromagnetic waves in this composite medium is due to the resonant behavior of the effective permittivity, while retardation in a CNT is caused by the localization of the guided waves to the CNT surface.

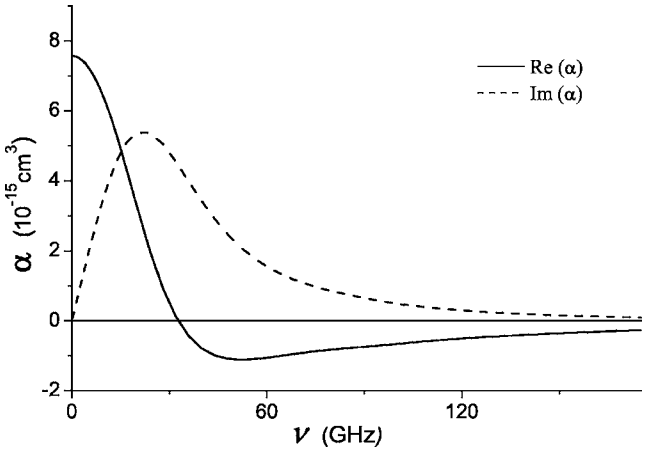

FIG. 5. Frequency dependences of the real (solid line) and imaginary (dashed line) parts of the polarizability scalar of a (23,0) semiconducting zigzag CNT of length $L=1$ μm.

At frequencies below the first geometric resonance, the real parts of the polarizability scalar of both semiconducting and metallic CNTs remain positive and tend to the polarizability scalar of a perfectly conducting cylinder as $\omega \to 0$. Note that this behavior does not account for the Coulomb screening of π electrons (see Ref. 5 for details), which is of importance in the low-frequency regime. Coulomb screening leads to the nonlocality of the CNT response, which was neglected for the derivation the boundary conditions (6)–(8) and is differently manifested in semiconducting and metallic CNTs. Thus, Coulomb screening distinguishes the actual electrostatic properties of semiconducting and metallic CNTs.

V. ANALYSIS AND DISCUSSION

A. Geometric resonances and CNT-based composite mediums

The geometric resonances can manifest themselves in the optical characteristics of CNT-based composite media.[51–56]. However, the length distributions of CNTs in the composite mediums studied are unknown and samples of the composite medium may differ in morphology, orientational statistics, etc. Thus, only a qualitative comparison of theoretical results for isolated CNTs with experimental data for CNT-based composite mediums is possible.

The main feature experimentally observed in Refs. 51–56 is a nonmonotonic frequency dependence of the reflectance and transmittance of slabs of CNT-based composite mediums in the spectral range 1–100 THz. This behavior does not follow from the standard Drude theory[57] and, until now, has not been given a satisfactory theoretical interpretation. Ugawa *et al.*[52] found empirically that the effective permittivity of a CNT-based composite medium can be represented as a superposition, of Drudian and Lorentzian functions, which allowed them to assume excitation in CNTs of low-frequency "Lorentz oscillations for the localized transitions." The spectral width of the resonance is of the order of the resonant frequency.[52] Obviously, it is then inappropriate to classify the composite medium's response as a "resonance."

Nevertheless, the experimentally observed broad low-frequency peak can be interpreted as a inhomogeneously broadened geometric resonance in an isolated CNT. Indeed, with realistic CNT parameters, the calculated magnitude of the first geometric resonance frequency ω_1 falls into the experimentally found spectral range. Furthermore, the magnitude of ω_1 is strongly influenced by the CNT length and type, as may be concluded from Figs. 4 and 5. Consequently, one can expect strong inhomogeneous broadening of the resonance due to distributions of the length and type of CNTs. Our theory predicts the isolated CNT spectral width to be approximately 50 times less than the resonance frequency ω_1. This means that the inhomogeneous broadening of the

Lorentz line can really dominate over all other possible broadening mechanisms—thermal broadening, in particular. That explains the temperature independence of experimental data obtained by Ugawa *et al.*[52] over a wide temperature range from 7.8 K to 298 K.

Measurements carried out in thin films containing CNTs aligned normal to the thickness direction [54,55] demonstrate strong optical anisotropy of films. The optical response for axially aligned incident electric field significantly exceeds the response for transverse alignment (i.e., $E_{0z}=0$). This fact is in complete agreement with the axial conductivity model used in our paper and resulted in the boundary conditions (6)–(8).

In the low-frequency regime ($\hbar\omega < 10^{-2}$ eV), measurements[53–55] show a rapid decrease of the polarizability scalar α as the frequency decreases. Such a behavior is in accordance with theoretical results presented in Figs. 4 and 5, and it is completely inconsistent with the Drude theory for bulk media, which predicts $\alpha \sim 1/\omega(\omega+i/\tau)$ in the low-frequency regime.[57] The reason is that the polarizability scalar of an isolated finite-length CNT—see (50)—with the axial current-density determined by (40) does not follow the Drude theory, but tends to follow that theory only as $L \to \infty$. Thus, the qualitative correlation between experimental observations and theoretical predictions allows us to recommend the approach developed for theoretical modeling of the optical response properties of CNT-based composite media in the framework of effective medium theories.[58]

B. CNTs as optical nanoantennas

The results obtained in this paper clearly demonstrate that CNTs can be used as antennas over the wide spectral range from terahertz to ultraviolet. Our theory of scattering by a CNT applies to the use of a CNT as a receiving antenna. Realistic antennas are characterized by several parameters,[36] all of which are dependent on the surface current density distribution. Therefore, (33), (34), and (40) constitute a mathematical technique for the calculation of the parameters of an isolated CNT of finite length as a receiving antenna.

The reciprocity theorem[59,60] allows us to extend our results and state the potential of isolated CNTs as transmitting nanoantennas. The scattering pattern is then referred to as the *radiation pattern*. The radiation pattern of an antenna during transmission and its reception pattern as a receiver are identical, the difference between transmitting and receiving antennas being in their power-handling capabilities. The transmitting antenna is also described by the same equations as the receiving antenna, but with E_{0z} replaced by a function describing the electromotive force (EMF). As Hanson[23] pointed out, the issue of the physical imposition of an EMF in a CNT is not entirely clear at present. One possible way is to apply a voltage to a CNT using epitaxially grown metallic contacts or semiconducting nanowires.[19] Another possibility is electromagnetic excitation using photoluminescence from quantum emitters placed inside the CNT. As examples of such quantum emitters, we suggest quantum dots; indeed, single quantum-dot excitation of a bowtie antenna has been realized.[46]

Under certain conditions, intrinsic defects and pinches in a CNT can also constitute quantum dots. This idea looks especially intriguing if applied to metallofullerenes encapsulated in a single-wall CNT (e.g., $[(\mathrm{Gd}@\mathrm{C}_{82})_n@\mathrm{SWNT}]$ peapods[61]), since such a structure places the metal atoms very close to the CNT surface and enables the invocation of the Purcell effect (a drastic decrease of the radiative lifetime).[7]

Probing of an electromagnetically excited CNT by a weak signal will allow electrical scanning of the radiation pattern. Such scanning in the field of radio-frequency antennas is carried out mechanically.

As noted in the predecessor papers,[20,23] CNT antennas are characterized by a low-level antenna efficiency $e_{\mathrm{eff}} = P_{\mathrm{out}}/P_{\mathrm{in}} \simeq 10^{-5}-10^{-6}$, where P_{in} and P_{out} denote the input and output powers, correspondingly. But this may be sufficient for CNT nanoantennas, because nanocircuits do not consume much power.[23] However, small values of e_{eff} lead to an increased noise temperature of the antennas, which could be deleterious for satisfactory performance.

Analysis of optical noise in a CNT optical nanoantenna constitutes a formidable and independent task to be considered elsewhere. Here, we are content to note that the analysis will require knowledge of the retarded Green function for the electromagnetic field in the presence of a CNT and the methodology developed in this paper can be used for that purpose. Specifically, the desired Green function is defined by the expressions (14) and (33) with

$$E_{0z}(z) = \left(\frac{\partial^2}{\partial z^2} + k^2\right)\frac{1}{2\pi}\int_0^{2\pi} \frac{\exp(ikr)}{r} d\phi, \tag{51}$$

where $r=[R^2+\rho_0^2-2R\rho_0\cos\phi+(z-z_0)^2]^{1/2}$ and ρ_0 and z_0 are cylindrical coordinates of the source.

Note also that not only CNTs can be used for the design of monomolecular carbon-based optical antennas. Carbon toruses[62] may serve as folded nanoantennas with a radiation pattern resembling that of a point magnetic dipole.

VI. CONCLUDING REMARKS

We presented here a theory of electromagnetic scattering by isolated, achiral, single-wall CNTs of finite length. The theory is applicable over a wide frequency range (from terahertz to ultraviolet) and especially in the vicinity of the plasmon resonance $\hbar\omega = 2\gamma_0$. The theory is based on a quantum-mechanical microscopic model of the conductivity of a CNT and the rigorous solution of electrodynamic boundary value problem for a finite-length CNT. The Leontovich-Levin equation for the induced surface current density was extended to CNTs and numerically solved. An approximate analytic solution was also found as the first step in an iteration process. The polarizability scalar of an isolated finite-length CNT in the low-frequency regime was evaluated and analyzed for potential use in estimating the effective constitutive properties of CNT-based composite media.[58] The resonances of strongly retarded surface waves caused by the edge effects (geometric resonances) were revealed. The radiation pattern of a CNT optical nanoantenna was calculated, and

some possibilities for pattern control were examined along with practical methods of exciting CNT nanoantennas. Thus, the analysis carried out in the paper forms a basis for the design and development of CNT nanoantennas in different frequency ranges.

ACKNOWLEDGMENTS

The research was partially supported by INTAS under Project No. 03-50-4409.

[1] S. Iijima, Nature (London) **354**, 56 (1991).
[2] *Carbon Nanotubes: Preparation and Properties*, edited by T. W. Ebbesen (CRC Press, Boca Raton, FL, 1997).
[3] M. S. Dresselhaus, G. Dresselhaus, and Ph. Avouris, *Carbon Nanotubes* (Springer, Berlin, 2001).
[4] G. Ya. Slepyan, S. A. Maksimenko, A. Lakhtakia, O. Yevtushenko, and A. V. Gusakov, Phys. Rev. B **60**, 17136 (1999).
[5] S. A. Maksimenko and G. Ya. Slepyan, in *Electromagnetic Fields in Unconventional Materials and Structures*, edited by O. N. Singh and A. Lakhtakia (Wiley, New York, 2000), pp. 217–255.
[6] S. A. Maksimenko and G. Ya. Slepyan, in *Nanometer Structures: Theory, modeling, and simulation*, edited by A. Lakhtakia (SPIE Press, Bellingham, WA, 2004), pp. 145–206.
[7] I. V. Bondarev, G. Ya. Slepyan, and S. A. Maksimenko, Phys. Rev. Lett. **89**, 115504 (2002).
[8] G. Ya. Slepyan, S. A. Maksimenko, V. P. Kalosha, J. Herrmann, E. E. B. Campbell, and I. V. Hertel, Phys. Rev. A **60**, R777 (1999).
[9] G. Ya. Slepyan, S. A. Maksimenko, V. P. Kalosha, A. V. Gusakov, and J. Herrmann, Phys. Rev. A **63**, 053808 (2001).
[10] G. Ya. Slepyan, A. A. Khrutchinski, A. M. Nemilentsau, S. A. Maksimenko, and J. Herrmann, Int. J. Nanosci. **3**, 343 (2004).
[11] O. V. Kibis, D. G. W. Parfitt, and M. E. Portnoi, Phys. Rev. B **71**, 035411 (2005).
[12] O. V. Kibis, S. V. Malevannyy, L. Hugget, D. G. W. Parfitt, and M. E. Portnoi, Electromagnetics **25**, 425 (2005).
[13] O. V. Kibis and M. E. Portnoi, Tech. Phys. Lett. **31**, 671 (2005).
[14] C. I. Wilke, W. Herrmann, and F. K. Kneubühl, Appl. Phys. B: Lasers Opt. **58**, 87 (1994).
[15] C. Fumeaux, J. Alda, and G. Boreman, Opt. Lett. **24**, 1629 (1999).
[16] C. Fumeaux, M. A. Gritz, I. Codreanu, W. L. Schaich, F. J. Gonzalez, and G. Boreman, Infrared Phys. Technol. **41**, 271 (2000).
[17] G. Ya. Slepyan, N. A. Krapivin, S. A. Maksimenko, A. Lakhtakia, and O. M. Yevtushenko, AEU, Int. J. Electron. Commun. **55**, 273 (2001).
[18] A. Jorio, A. G. Souza Filho, V. W. Brar, A. K. Swan, M. S. Unlu, B. B. Goldberg, A. Righi, J. H. Hafner, C. M. Lieber, R. Saito, G. Dresselhaus, and M. S. Dresselhaus, Phys. Rev. B **65**, 121402(R) (2002).
[19] A. Kazunori, M. Chikara, K. Hirotsugu, W. Hiroyuki, and S. Masaaki, U.S. Patent WO03083993 (10 September 2003).
[20] P. J. Burke, S. Li, and Z. Yu, cond-mat/0408418 (unpublished).
[21] M. S. Dresselhaus, Nature (London) **432**, 959 (2004).
[22] Y. Murakami, E. Einarsson, T. Edamura, and S. Maruyama, Phys. Rev. Lett. **94**, 087402 (2005).
[23] G. W. Hanson, IEEE Trans. Antennas Propag. **53**, 3426 (2005).
[24] Y. Wang, K. Kempa, B. Kimball, G. Benham, W. Z. Li, T. Kempa, J. Rybczynski, A. Herczynski, and Z. F. Ren, Appl. Phys. Lett. **85**, 2607 (2004).
[25] Z. Yu, S. Li, and P. J. Burke, Chem. Mater. **16**, 3414 (2004).
[26] S. Li, Z. Yu, C. Rutherglan, and P. J. Burke, Nano Lett. **4**, 2003 (2004).
[27] A. Lakhtakia, G. Ya. Slepyan, S. A. Maksimenko, O. M. Yevtushenko, and A. V. Gusakov, Carbon **36**, 1833 (1998).
[28] F. J. Garcia-Vidal, J. M. Pitarke, and J. B. Pendry, Phys. Rev. Lett. **78**, 4289 (1997).
[29] W. Lu, J. Dong, and Z.-Ya. Li, Phys. Rev. B **63**, 033401 (2000).
[30] L. A. Weinstein, *The Theory of Diffraction and the Factorization Method* (Golem, New York, 1969).
[31] R. Mittra and S. W. Lee, *Analytical Techniques in the Theory of Guided Waves* (Macmillan, New York, 1971).
[32] G. Sinclair, E. C. Jordan, and E. W. Vaughan, J. Br. Inst. Radio Eng. **35**, 1451 (1947).
[33] A. Lakhtakia, Microwave Opt. Technol. Lett. **7**, 328 (1994).
[34] A. Lakhtakia, in *Advanced Electromagnetism—Foundations, theory and applications*, edited by T. W. Barrett and D. M. Grimes (World Scientific, Singapore, 1995), pp. 390–410.
[35] M. A. Leontovich and M. L. Levin, Int. J. Theor. Phys. **14**, 481 (1944).
[36] C. A. Balanis, *Antenna Theory: Analysis and design* (Wiley, New York, 1997).
[37] E. Hallén, Nova Acta Regiae Soc. Sci. Ups. **11**, 1 (1938).
[38] J. van Bladel, *Electromagnetic Fields* (Hemisphere, Washington, DC, 1985).
[39] A. S. Ilyinsky, G. Ya. Slepyan, and A. Ya. Slepyan, *Propagation, Scattering and Dissipation of Electromagnetic Waves* (Peter Peregrinus, London, 1993).
[40] D. L. Carroll, P. Redlich, P. M. Ajayan, J. C. Charlier, X. Blase, A. De Vita, and R. Car, Phys. Rev. Lett. **78**, 2811 (1997).
[41] J. W. G. Wildoer, L. C. Venema, A. G. Rinzler, R. E. Smalley, and C. Dekker, Nature (London) **391**, 59 (1998).
[42] H. C. Pocklington, Proc. Cambridge Philos. Soc. **9**, 324 (1897).
[43] A. Lakhtakia, *Beltrami Fields in Chiral Media* (World Scientific, Singapore, 1994).
[44] $v_F = 3\gamma_0 b/2\hbar = 9.71 \times 10^5$ m/s (see Ref. 5).
[45] M. F. Lin and Kenneth W.-K. Shung, Phys. Rev. B **50**, R17744 (1994).
[46] J. N. Farahani, D. W. Pohl, H.-J. Eisler, and B. Hecht, Phys. Rev. Lett. **95**, 017402 (2005).
[47] H. C. van de Hulst, *Light Scattering by Small Particles* (Dover, New York, 1981).
[48] O. Hilt, H. B. Brom, and M. Ahlskog, Phys. Rev. B **61**, R5129 (2000).
[49] S. A. Maksimenko, G. Ya. Slepyan, V. P. Kalosha, N. N. Ledentsov, A. Hoffman, and D. Bimberg, Mater. Sci. Eng., B **82**, 215 (2001).
[50] H. Ajiki, T. Tsuji, K. Kawano, and K. Cho, Phys. Rev. B **66**, 245322 (2002).

[51] F. Bommeli, L. Degiorgi, P. Wachter, W. S. Bacsa, W. A. de Heer, and L. Forro, Synth. Met. **86**, 2307 (1997).
[52] A. Ugawa, A. G. Rinzler, and D. B. Tanner, Phys. Rev. B **60**, R11305 (1999).
[53] B. Ruzicka, L. Degiorgi, R. Gaal, L. Thien-Nga, R. Bacsa, J. P. Salvetat, and L. Forro, Phys. Rev. B **61**, R2468 (2000).
[54] T.-I. Jeon, K. J. Kim, C.-J. Oh, J.-H. Son, K. H. An, D. J. Bae, and Y. H. Lee, Appl. Phys. Lett. **80**, 3403 (2002).
[55] T.-I. Jeon, K. J. Kim, C. Kang, I. H. Maeng, J.-H. Son, K. H. An, J. Y. Lee, and Y. H. Lee, J. Appl. Phys. **95**, 5736 (2004).
[56] J. Wu and L. Kong, Appl. Phys. Lett. **84**, 4956 (2004).
[57] C. Kittel, *Introduction to Solid State Physics*, 4th ed (Wiley Eastern, New Delhi, India, 1971).
[58] *Selected Papers on Linear Optical Composite Materials*, edited by A. Lakhtakia (SPIE Press, Bellingham, WA, 1996).
[59] V. H. Rumsey, Phys. Rev. **94**, 1483 (1954).
[60] R. F. Harrington, *Time-Harmonic Electromagnetic Fields* (McGraw-Hill, New York, 1961).
[61] K. Hirahara, K. Suenaga, S. Bandow, H. Kato, T. Okazaki, H. Shinohara, and S. Iijima, Phys. Rev. Lett. **85**, 5384 (2000).
[62] M. F. Lin, Phys. Rev. B **58**, 3629 (1998).